A Tribological Study on NAB-Y_2O_3-CNT Composite prepared by the Powder Metallurgy Method

Shahad Ali Hammood
Materials Engineering College, Metallurgical Engineering Department, University of Babylon, Iraq
shahad.alkawaz@uobabylon.edu.iq (corresponding author)

Kawthar Yahya Al-Dulaimi
Materials Engineering College, Metallurgical Engineering Department, University of Babylon, Iraq
mat.kawthar.y@uobabylon.edu.iq

Haydar Al-Ethari
Materials Engineering College, Metallurgical Engineering Department, University of Babylon, Iraq
dr.eng.alethari@uobabylon.edu.iq

Received: 15 June 2024 | Revised: 13 July 2024 | Accepted: 16 July 2024

 DOI: https://doi.org/10.48084/etasr.8150

ABSTRACT

Nickel Aluminum Bronze (NAB) alloys display characteristics like superior strength and excellent wear resistance. In this work, NAB was reinforced using various volume fractions of yttrium (Y_2O_3) and/or carbon nanotube (CNT) particles prepared using the Powder Metallurgy (PM) method. General full factorial design was used in MiniTab19 software. The experimental results showed a significant influence of the Y_2O_3 and CNT particles on mechanical and physical properties. The optimal results were recorded for the sample having 6 vol.% of Y_2O_3 and 1.5 vol.% of CNT. This sample exhibited the highest effect on characteristics with hardness value of 288 Hv, porosity of 10.2%, surface roughness of 0.15 µm, average particle size of 37.55 µm, wear rate of 0.0000313 g/mm, and friction coefficient of 0.68. The results demonstrated that there is an improvement of 64% in microhardness in comparison with the base alloy. Porosity, surface roughness, wear rate, friction coefficient, and average grain size were reduced by 4%, 81%, 71%, 31%, and 24%, respectively.

Keywords-nickel aluminum bronze; powder metallurgy; yttrium; carbon nanotube; general full factorial

I. INTRODUCTION

One type of copper-aluminum alloy is the Nickel-Aluminum Bronze (NAB) alloy which has been used extensively to produce a wide range of components for the oil and gas, automotive, aerospace, and marine industries due to its good corrosion resistance, mechanical qualities, and resistance to wear and galling. NAB alloys are castable, heat treatable, and weldable [1, 2]. The heavy oxide layer that typically forms on their surfaces is what gives them their exceptional corrosion resistance. Because NAB alloys do not undergo brittle transition at lower temperatures, they may maintain their mechanical qualities, which is why the oil and gas and maritime sectors use them extensively in cryogenic conditions [3]. They are widely employed in the fabrication of wind flap bearings, window frames, aviation landing gear, propellers, valves, and winch gear. The extensive utilization of the NAB alloy system can be attributed to its complex microstructure and chemical composition, which contribute to the alloy's enhanced characteristics [4]. The characteristics of NAB materials are primarily influenced by their microstructure and micro constituents. The typical microstructure of a NAB alloy consists of multiple intermetallic Kappa phases (K_I, K_{II}, K_{III}, and K_{IV}) and copper-rich α, β' phases (martensitic). In intermetallic Kappa phases, phases K_I, K_{II}, K_{III}, and K_{IV} indicate rosette, globular, lamellar, and fine globular forms, respectively [5]. The microstructure of NAB alloy undergoes several modifications even at equilibrium cooling rates. When the liquid solidifies, it first forms a single-phase β structure. Later, when the material cools down even more, the α phase precipitates into grains from the boundaries, forming a Widmanstatten structure [6]. If it was cooled much further, the iron-rich K_I phase would precipitate out of the rosette structure. Furthermore, at lower temperatures, the K_{II} and K_{III} phases are produced from inside grains. Finally, tiny K_{IV} phase particles precipitate [7, 8].

Few studies in the past have examined the mechanical and physical characteristics of NAB alloys through the application of the Powder Metallurgy (PM) method. Authors in [9]

prepared NAB strengthened with varying percentages of Cubic Boron Nitride (CBN) particles and studied their effect on the base alloy's mechanical, elastic, and physical characteristics. Authors in [10] studied the influence of heat treatment on the microstructure and microhardness of NAB alloys. Authors in [11] compared cast [$Cu_{10}Al_5Ni_5Fe$] NAB alloy with cast in situ Aluminum Bronze (AB)-TiC [$(Cu_{10}Al_3Fe)_5TiC$] composite considering the physical, mechanical, and sliding wear characteristics. Authors in [12] investigated the impact of Ti on the mechanical characteristics, corrosion behavior, and microstructure of a specific NAB alloy, $CuAl_{10}Fe_5Ni_5$ (C95500), and compared the results with the ones of the Ti-free NAB alloy.

The present work studies the influence of Y_2O_3 and/or CNT particles on the microstructure, porosity, hardness, Surface Roughness (SR-Ra), grain size, Friction Coefficient (FC), and Wear Rate (WR) of the NAB alloy. The optimum percentages were found using the full factorial method based on the above-mentioned properties.

II. EXPERIMENTAL PART

A. Utilized Powders

Table I displays the materials utilized in this work to prepare the NAB alloys.

TABLE I. PURITY AND AVERAGE PARTICLE SIZE OF THE USED POWDERS

Powder	Purity	Avg. particle size	Source
Copper	99.10	18.90 µm	BDH Chemicals Ltd Poole England
Aluminum	98.90	20 µm	BDH Chemicals Ltd Poole England
Iron	99.28	8.949 µm	BDH Chemicals Ltd Poole England
Nickel	99.11	23.35 µm	Gentral drug house (P) Ltd.India
Yttrium	98.99	4.518 µm	BDH Chemicals Ltd Poole England
CNT	99	40.50 nm	Nanjing nanotechnology

B. Sample Preparation

According to ASTM B150, samples of the base NAB alloy, with a chemical composition of 82% Cu-9% Al-5% Ni - 4% Fe [13] were prepared using the PM method. Several samples were prepared with different volume fractions of CNT and Y_2O_3. Wet mixing with acetone (2 wt%) for 6 h in an electric mixture type (Lab pot mill STGQM-1/5-2) was used.

The samples were compacted using a double action die that was specially designed to prepare cylindrical samples with a diameter of 15 mm and a height of 3 mm at room temperature via an electric hydraulic press type CT340-CT440. The samples were utilized in microstructure, hardness, porosity, SR, WR, and grain size tests. A compacting pressure of 700 MPa determined experimentally based on the highest green density was used to prepare the green compacts. The green compacts were sintered using a vacuum high-temperature tube furnace operating at a pressure of 10^{-4} torr. Two steps were taken in the sintering program, which involved heating at a rate of 10 °C/min for 90 min at 630 °C and 90 min at 930 °C. The samples were left to cool down inside the furnace. The sintered samples were heat treated for 50 min at a rate of 10 °C/min to 900 °C, quenched in ice water, and then tempered for 30 min at 500 °C [14].

C. Design of the Experiments

A statistical strategy for designing experiments is the General Full Factorial Design (GFFD). Its primary objective is to look into the main influences and interactions of factors (studied parameters) at various levels [15]. The statistical software package Minitab 19 was used to examine the effects of the volume fraction percentage of yttrium (Y_2O_3) and the contents of CNT at four different levels: 0, 2, 4, and 6 vol.% for Y_2O_3 and 0, 0.5, 1, and 1.5 vol.% for CNT. The obtained design of experiments is illustrated in Table II.

TABLE II. RESULTS OF THE EXPERIMENT DESIGN BY THE GENERAL FULL FACTORIAL DESIGN METHOD

Std Order	Y_2O_3 content vol.%	CNT content vol.%	Sample code
1	0	0	BA
2	0	0.5	A_1
3	0	1	A_2
4	0	1.5	A_3
5	2	0	A_4
6	2	0.5	A_5
7	2	1	A_6
8	2	1.5	A_7
9	4	0	A_8
10	4	0.5	A_9
11	4	1	A_{10}
12	4	1.5	A_{11}
13	6	0	A_{12}
14	6	0.5	A_{13}
15	6	1	A_{14}
16	6	1.5	A_{15}

III. MATERIAL ASSESSMENT

The effect of the Y_2O_3 and the CNT was evaluated by five response parameters. These parameters are porosity, hardness, SR, WR, and grain size of the prepared samples. The samples (15 mm in diameter and 3 mm in height), were appropriately ground and polished using paper grits of 180, 220, 400, 600, 800, 1000, 1200, 2000, and 2500 µm [16]. A grinding and polishing machine was used for this process, then the samples were etched at room temperature with a solution consisting of (5 g $FeCl_3$, 2 mL HCl, and 95 mL C_2H_5OH) [17]. An electric dryer was used to dry all the samples after washing them in distilled water. To capture the sample's microstructure, a 1280 XEQMM300TUSB optical microscope was utilized. Equation (1) was used to measure the porosity of the final (heat-treated) samples by ASTM B-328 [18]:

$$Porosity\ (Apparent)\% = \frac{W_w - W_d}{W_{sat} - W_s} \times 100 \qquad (1)$$

where W_d is the sample's dry weight (g), W_w is the sample's wet weight (weighted following a 24-h immersion in distilled water) (g), W_{sat} is the saturated weight (the sample was weighed after being submerged in pure water at 80°C for 5 h) (g), W_s represents the suspended weight (weight of the sample suspended in distilled water) (g).

A Vickers micro-hardness device type (TH 717) was used to perform the hardness test for the prepared samples. A load of 500 g applied for 10 s with a square base diamond pyramid was used for every specimen, and the average of three measurements was considered to record the hardness. After

preparing the samples, a SR tester (TR200 hand-held roughness tester, model TA620 Stan & Co) was used to measure the SR. Before the test, the surface of the samples was ground and the roughness value was recorded (0.15 µm). Pin-on-disc testing method according to ASTMG99 was used to investigate sliding wear and FC. The initial weight of the sample was measured (w_o). Each sample was inserted in the holder, making certain that its end surface was parallel to the disk surface. The holder was adjusted to get a desirable wear track radius of 5 mm. The load was 20 N with a rotation speed of 250 rpm. The test took 30 min to complete. The wear rate is determined by [19]:

$$R.W = \frac{\Delta W}{2\pi r t} \quad (2)$$

where $R.W$ is the wear rate (g/mm), ΔW is the weight loss (g), or the difference between sample weight before and after the test, t is the sliding time (min), r is the sample's radius to the disc' center (5 mm).

Grain size analysis was measured by the ImageJ program version 1.8.0 after obtaining the microstructure images by the optical microscope.

IV. RESULTS AND DISCUSSION

A. Microstructure Analysis

The microstructures of some of the sintered and heat-treated samples are depicted in Figure 1, with an image width of 80 µm. Figure 1 shows the resulting microstructure of the samples BA, A_1, A_3, A_4, A_{12}, and A_{15} after quenching in water. Because of the high cooling rate that causes β to shift, martensite is visible as fine black lines or nodular martensite. The α-phase is represented by the displayed white regions in the microstructure.

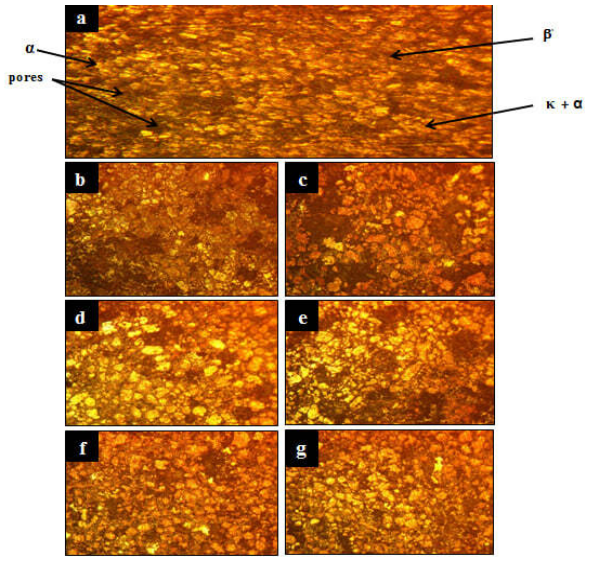

Fig. 1. Microstructure of (400 X magnification): (a) BA, (b) A_1, (c) A_3, (d) A_4, (e) A_5, (f) A_{12}, and (g) A_{15} samples.

B. Hardness and Porosity Tests

Vickers micro-hardness and porosity are shown in Figures 2 and 3 for all prepared samples after heat treatment.

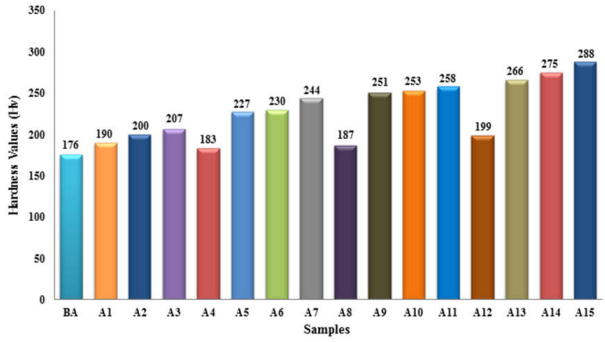

Fig. 2. Microhardness of the samples prepared in this study.

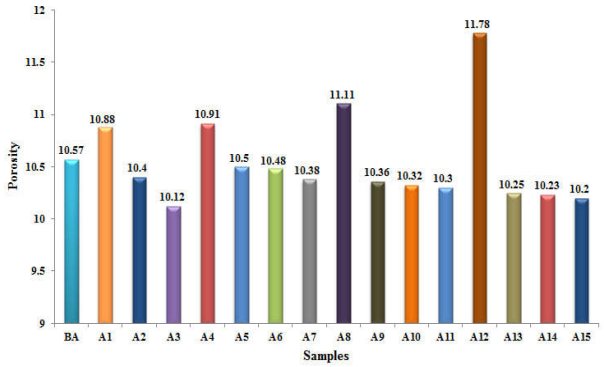

Fig. 3. Porosity of the prepared samples.

The base alloy's recorded hardness was 176 HV, in accordance with [20]. The hardness increased dramatically as the fraction of Y_2O_3 increased. This increase may be caused by the high hardness of the Y_2O_3 particles, which tend to inhibit matrix movement and function as barriers to dislocation motion, but increases the porosity of the base alloy due to the large particle size of Y_2O_3. CNT increased the base alloy's hardness and decreased its porosity due to its very small size and its nature as a hard reinforcing phase. An addition of 0.5 vol% CNT increased the porosity due to the heterogeneous distribution throughout the base alloy (CNT agglomerates result in a greater plastic strain in their vicinity and promote the formation of voids). The base alloy's porosity decreased and its hardness increased when CNT and Y_2O_3 were added.

C. Gain Size Test

Figure 4 displays the results of the average grain size. Samples containing yttrium exhibited a higher average grain size than samples containing CNT. Samples with yttrium and CNT have a lower average grain size than the other samples. The lowest average grain size is was observed in sample A_{15}.

D. Wear Test

Figures 5-7 show the results of SR, FC, and WR for all prepared samples. Samples containing yttrium have lower SR, WR, and FC values than the base alloy due to the high hardness of the yttrium. The samples with CNT had lower SR, RW, and FC than the sample containing Y_2O_3. Samples combining CNT and Y_2O_3 gave the best results. Sample A_{15} exhibited the lowest SR, WR, and FC. Table III displays the results of the physical and mechanical tests.

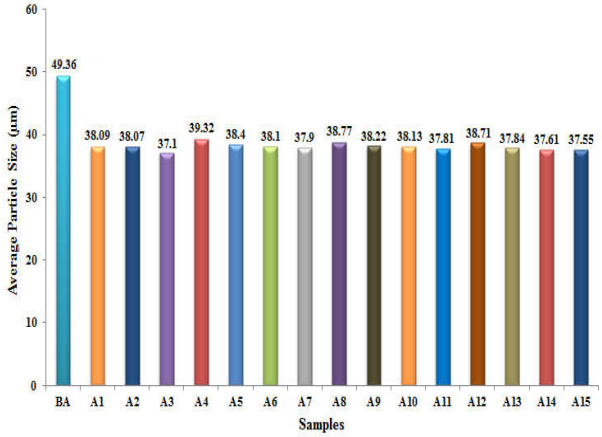

Fig. 4. The average grain size of the prepared samples.

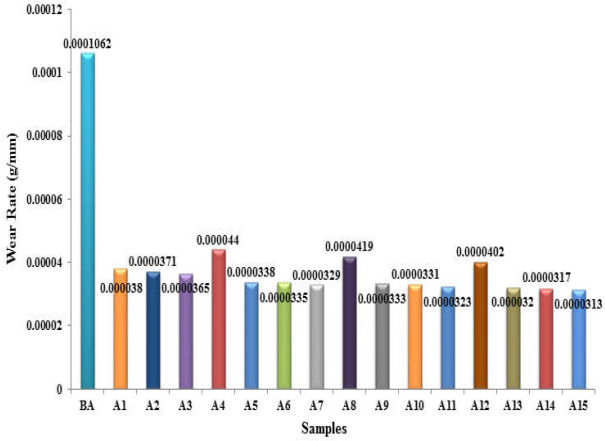

Fig. 6. The wear rate of the prepared samples.

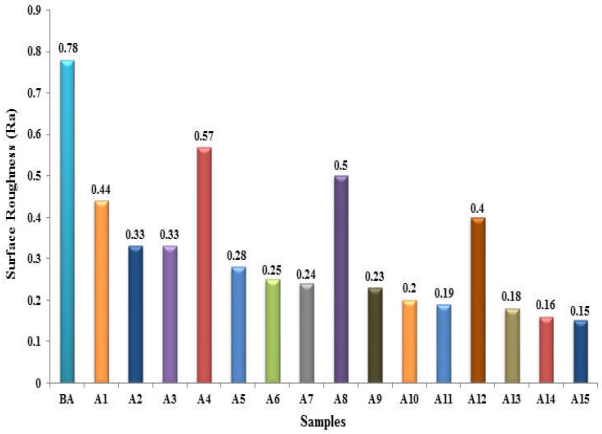

Fig. 5. Surface roughness of the prepared samples.

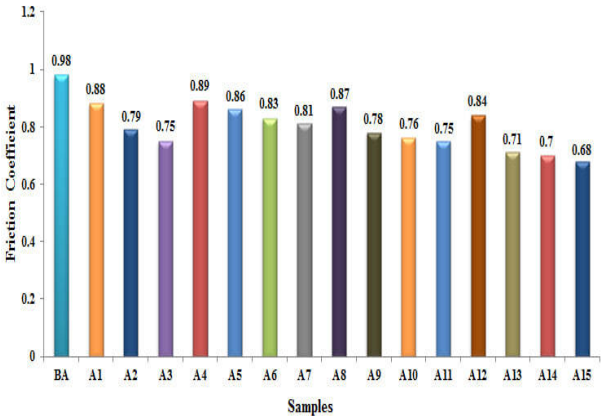

Fig. 7. Friction coefficient of the prepared samples.

TABLE III. RESULTS OF MECHANICAL AND PHYSICAL TESTS

Sample	Y_2O_3 vol.%	CNT vol.%	Hardness value (Hv)	Porosity %	SR (µm)	WR (g/mm)	FC	Avg. grain size (µm)
BA	0	0	176	10.57	0.78	0.0001062	0.98	49.36
A_1	0	0.5	190	10.88	0.44	0.000038	0.88	38.09
A_2	0	1	200	10.4	0.33	0.0000371	0.79	38.07
A_3	0	1.5	207	10.12	0.33	0.0000365	0.75	37.1
A_4	2	0	183	10.91	0.57	0.000044	0.89	39.32
A_5	2	0.5	227	10.5	0.28	0.0000338	0.86	38.4
A_6	2	1	230	10.48	0.25	0.0000335	0.83	38.1
A_7	2	1.5	244	10.38	0.24	0.0000329	0.81	37.9
A_8	4	0	187	11.11	0.5	0.0000419	0.87	38.77
A_9	4	0.5	251	10.36	0.23	0.0000333	0.78	38.22
A_{10}	4	1	253	10.32	0.2	0.0000331	0.76	38.13
A_{11}	4	1.5	258	10.3	0.19	0.0000323	0.75	37.81
A_{12}	6	0	199	11.78	0.4	0.0000402	0.84	38.71
A_{13}	6	0.5	266	10.25	0.18	0.000032	0.71	37.84
A_{14}	6	1	275	10.23	0.16	0.0000317	0.7	37.61
A_{15}	6	1.5	288	10.2	0.15	0.0000313	0.68	37.55

E. Factorial Design Analysis

Figures 8-13 represent the main effects and interaction plots for hardness, porosity, SR, average particle size, WR, and FC results which display the effect of the addition of Y_2O_3 and CNT to the prepared samples. The ability to examine how variables interact is one of the main advantages of factorial design. The interaction term may often be more significant than the primary effects (the effects of factors taken individually) in many cases [21, 22]. Figures 8-13 show that the sample with CNT had better results than the samples with Y_2O_3. When the data distribution is normal, the normal probability plot demonstrates that points fall quite near a straight line as shown in Figure 14. The normal probability plot of the residuals can be used to examine the data's normality.

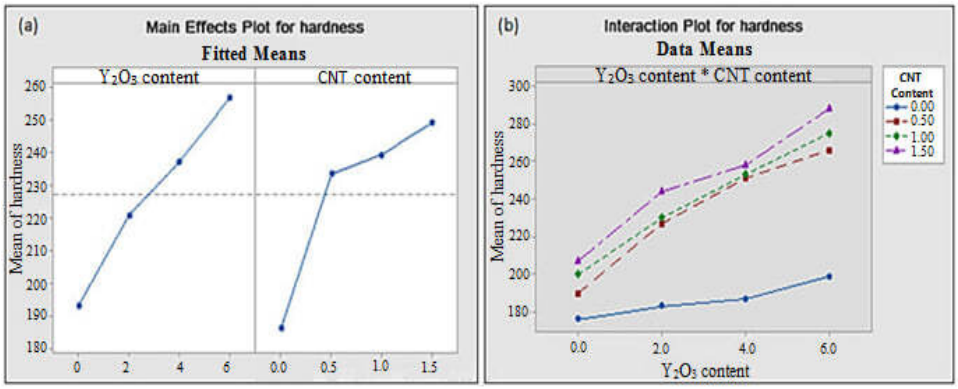

Fig. 8. (a) Main effects plot for hardness, (b) interaction plot for hardness.

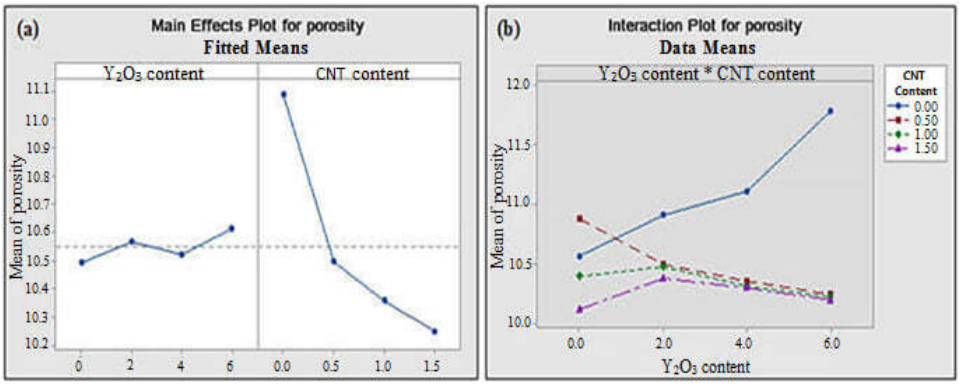

Fig. 9. (a) Main effects plot for porosity, (b) interaction plot for porosity.

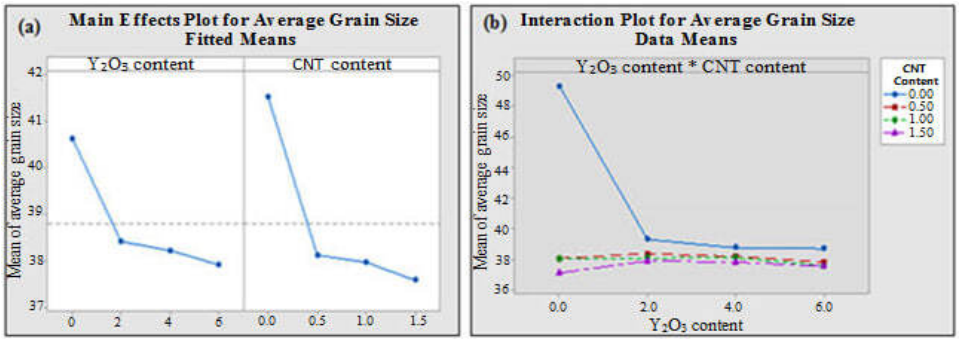

Fig. 10. (a) Main effects plot for average grain size, (b) interaction plot for average grain size.

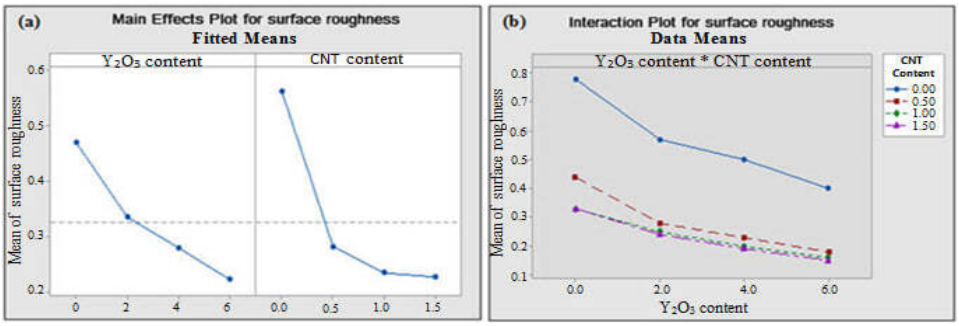

Fig. 11. (a) Main effects plot for surface roughness, (b) interaction plot for surface roughness.

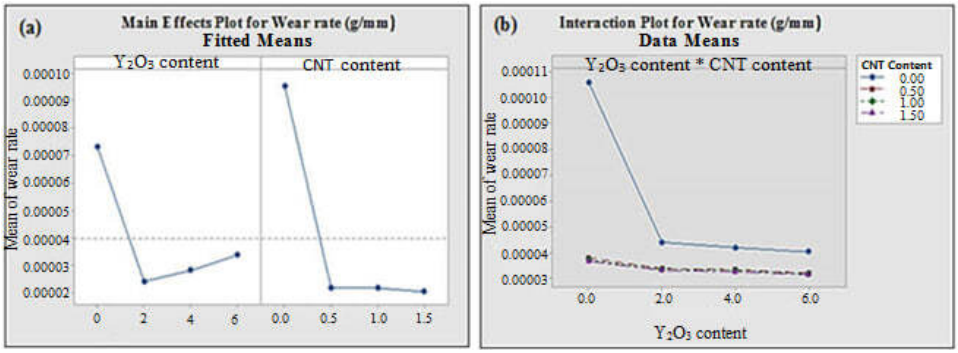

Fig. 12. (a) Main effects plot for wear rate, (b) interaction plot for wear rate.

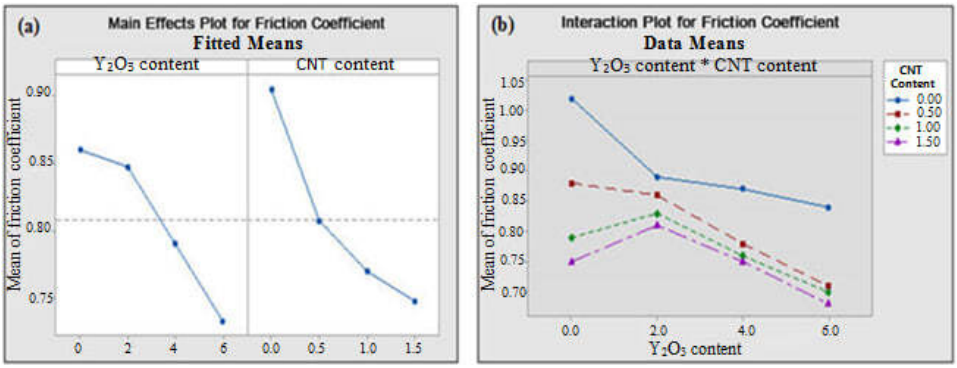

Fig. 13. (a) Main effects plot for friction coefficient, (b) interaction plot for friction coefficient.

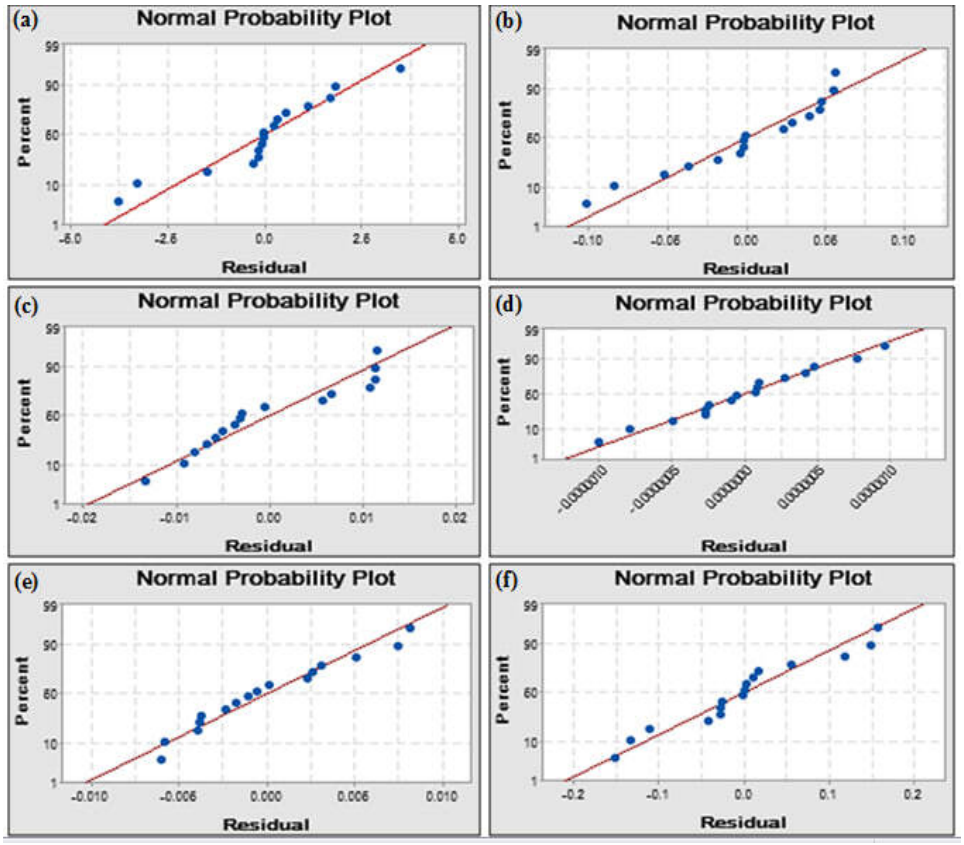

Fig. 14. Normal probability plot for: (a) hardness, (b) porosity, (c) SR, (d) WR, (e) FC, and (f) grain size values.

To compare the relative magnitudes and statistical significance of the main and interaction influences, a Pareto chart of the standardized influences can be utilized.

- When there is no error term in the model, the chart illustrates the absolute value of the unstandardized influences.
- If there is an error term in the model, the chart illustrates the absolute value of the standardized influences.

The standardized influences are plotted by Minitab according to decreasing absolute values as shown in Figures 15-20. The chart's reference line indicates which influences are significant. Minitab draws the reference line at a significance level of 0.05 by default. Minitab draws the reference line using Lenth's approach, which has no error term. In these results, all four major influences have statistical significance ($\alpha = 0.05$) [23]. These important influences primarily consist of two influences: CNT content (B) and Y_2O_3 (A). Furthermore, you can observe that the CNT content (B), which extends the farthest, has the largest influence.

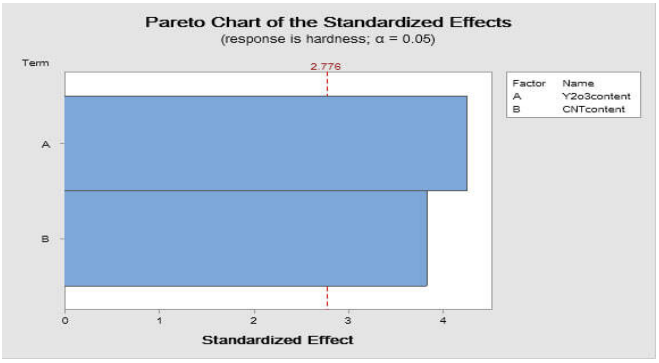

Fig. 15. Pareto chart of the standardized influences for the hardness test.

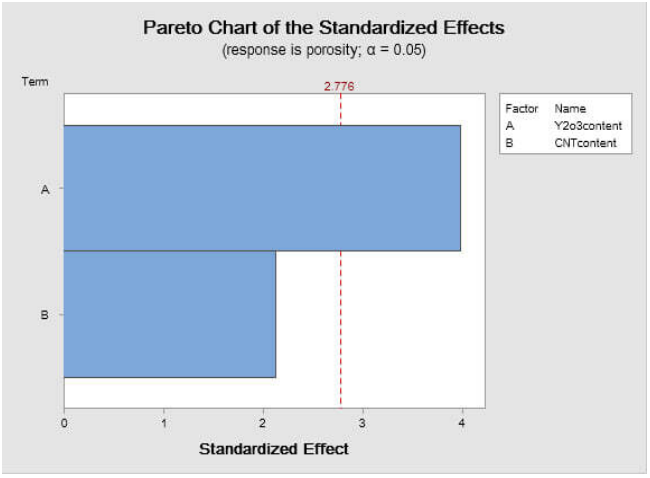

Fig. 16. Pareto chart of the standardized influences for the porosity test.

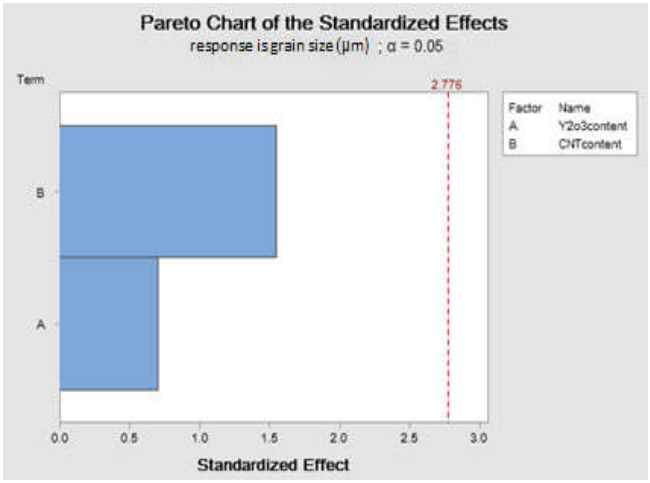

Fig. 17. Pareto chart of the standardized influences for the average grain size.

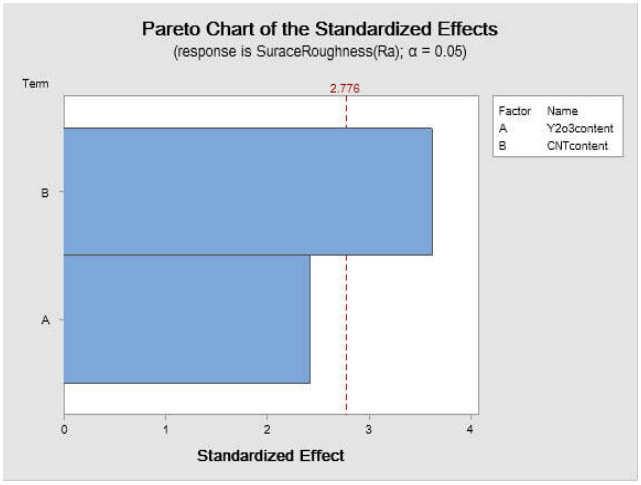

Fig. 18. Pareto chart of the standardized influences for surface roughness.

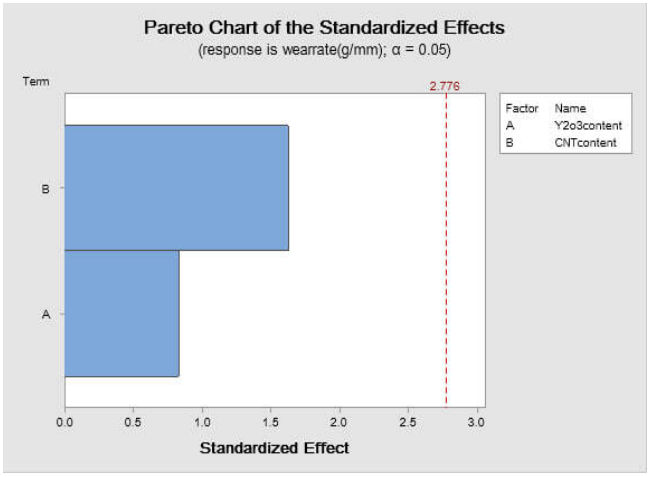

Fig. 19. Pareto chart of the standardized influences for wear rate.

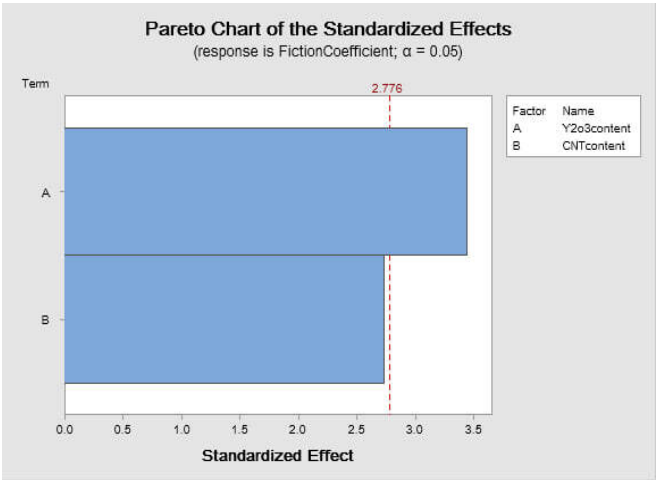

Fig. 20. Pareto chart of the standardized influences for friction coefficient.

The response optimizer can be used to optimize the desired formulation based on different process variables. Composite desirability (D) is another statistical measure that can be used to confirm the accuracy of the optimization plot [24]. When D exceeds 0.90, this indicates that the factors and responses optimized through statistical analysis are extremely accurate and dependable. The optimal sample represents A_{15}, which has the highest hardness, lowest porosity, SR and grain size, WR, and FC. The optimization plot for the desired responses is displayed in Figure 21.

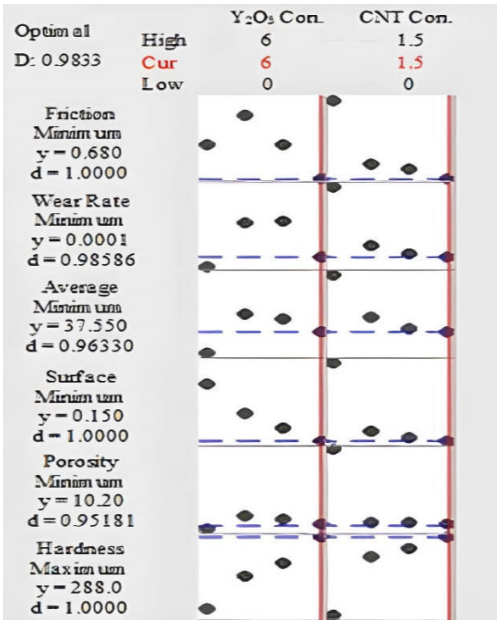

Fig. 21. Response optimization results.

V. CONCLUSIONS

During the recent years, there has been an increase in the demand for innovative materials with outstanding mechanical and tribological qualities for various industrial applications. NAB alloys are used extensively due to their superior strength, corrosion resistance, and resistance to wear. For even more demanding applications, greater advancements in these qualities are desired. The objective of this study was to determine the effects of yttrium oxide (Y_2O_3) and/or carbon nanotube (CNT) particles on the physical properties (porosity and surface roughness), tribological properties (wear resistance and friction coefficient), mechanical properties (hardness), and microstructure of NAB alloy that was fabricated via the powder metallurgy method. Based on the results, the following conclusions are made:

1. Reinforcing the NAB alloy by 6 vol.% of Y_2O_3 and 1.5 vol. % of CNT gave a higher hardness than the other reinforcing percentages. Porosity, surface roughness, wear rate, friction coefficient, and average grain size of the alloy reinforced with the mentioned volume fraction are less than those of the base alloy by 4%, 81%, 71%, 31%, and 24%, respectively.
2. Adding CNT increases the hardness of the base alloy more than adding Y_2O_3.
3. The porosity of the base alloy is increased by the addition of Y_2O_3.
4. Adding Y_2O_3 and CNT together improves the properties of the base alloy more than adding Y_2O_3 and CNT separately.

The novelty of this work lies in the exploration of the combined effect of Y_2O_3 and CNT additions on NAB properties using powder metallurgy. In contrast to previous studies that concentrate on discrete reinforcements such as heat treatment or addition of Cubic Boron Nitride (CBN), this work presents a novel composite strategy that shows promise for obtaining better mechanical and tribological performances.

These findings suggest that the combined reinforcement of Y_2O_3 and CNTs offers a promising approach to enhancing the performance of NAB alloys. Subsequent studies could examine how to optimize the ratios of reinforcement and explore how these composites behave tribologically under different wear conditions.

ACKNOWLEDGMENTS

The authors wish to acknowledge the help of all the staff of the Material Engineering College, Metallurgical Engineering Department, University of Babylon, Iraq, for their invaluable assistance during the experimental activities.

REFERENCES

[1] S. L. Song, D. G. Li, D. R. Chen, and P. Liang, "The role of Ti in cavitation erosion and corrosion behaviours of NAB alloy in 3.5 % NaCl solution," *Journal of Alloys and Compounds*, vol. 919, Oct. 2022, Art. no. 165728, https://doi.org/10.1016/j.jallcom.2022.165728.

[2] A. Shahriari, D. Chalasani, B. S. Amirkhiz, and M. Mohammadi, "Corrosion performance of wire arc additively manufactured NAB alloy," *npj Materials Degradation*, vol. 7, no. 1, Oct. 2023, Art. no. 85, https://doi.org/10.1038/s41529-023-00405-x.

[3] D. G. Li, S. L. Song, D. R. Chen, and P. Liang, "Effects of Ce, Sm and Yb on cavitation erosion of NAB alloy in 3.5% NaCl solution," *Ultrasonics Sonochemistry*, vol. 88, Aug. 2022, Art. no. 106093, https://doi.org/10.1016/j.ultsonch.2022.106093.

[4] A. M. Okoro, S. S. Lephuthing, L. Rasiwela, and P. A. Olubambi, "Nondestructive measurement of the mechanical properties of graphene nanoplatelets reinforced nickel aluminium bronze composites," *Heliyon*, vol. 7, no. 9, Sep. 2021, Art. no. e07978, https://doi.org/10.1016/j.heliyon.2021.e07978.

[5] B. Zhang, J. Wang, and F. Yan, "Load-dependent tribocorrosion behaviour of nickel-aluminium bronze in artificial seawater," *Corrosion Science*, vol. 131, pp. 252–263, Feb. 2018, https://doi.org/10.1016/j.corsci.2017.11.028.

[6] X. Chen *et al.*, "Influence of cutting speed on fretting wear properties of UVAM-processed NAB alloy," *Materials Characterization*, vol. 185, Mar. 2022, Art. no. 111711, https://doi.org/10.1016/j.matchar.2021.111711.

[7] S. Poojary, V. Marakini, R. N. Rao, and V. Vijayan, "Enhancing microstructure and mechanical properties of nickel aluminium bronze alloy through tin addition," *Scientific Reports*, vol. 13, no. 1, Oct. 2023, Art. no. 16907, https://doi.org/10.1038/s41598-023-44146-y.

[8] K. Morshed-Behbahani, A. J. Rayner, D. P. Bishop, and A. Nasiri, "Perspectives on the unusual electrochemical corrosion of Nickel Aluminum Bronze (NAB) alloy fabricated through laser-powder bed fusion additive manufacturing," *Corrosion Science*, vol. 228, Mar. 2024, Art. no. 111846, https://doi.org/10.1016/j.corsci.2024.111846.

[9] H. Al-Ethari and A. Jaafar, "Influence of Cubic Boron Nitride on the Physical and Mechanical Properties of NAB Alloy Prepared by Powder Matallurgy.," *Journal of Engineering and Applied Sciences*, vol. 13, pp. 874–879, Mar. 2018, https://doi.org/10.3923/jeasci.2018.874.879.

[10] Y. Lv, L. Wang, X. Xu, and W. Lu, "Effect of Post Heat Treatment on the Microstructure and Microhardness of Friction Stir Processed NiAl Bronze (NAB) Alloy," *Metals*, vol. 5, no. 3, pp. 1695–1703, Sep. 2015, https://doi.org/10.3390/met5031695.

[11] S. Rathod, Y. Srivastava, V. R. Kiragi, and A. Patnaik, "Evaluation of physical, mechanical and sliding wear properties of in-situ AB-TiC composite: a comparison with NAB alloy," *Engineering Research Express*, vol. 5, no. 2, Feb. 2023, Art. no. 025041, https://doi.org/10.1088/2631-8695/acd435.

[12] P. J. Rivero, C. Berlanga, J. F. Palacio, and M. V. Biezma-Moraleda, "Effect of Ti on Microstructure, Mechanical Properties and Corrosion Behavior of a Nickel-Aluminum Bronze Alloy," *Materials Research*, vol. 24, no. 2, Apr. 2021, Atr. no. e20200335, https://doi.org/10.1590/1980-5373-MR-2020-0335.

[13] S. M. Orzolek, J. K. Semple, and C. R. Fisher, "Influence of processing on the microstructure of nickel aluminum bronze (NAB)," *Additive Manufacturing*, vol. 56, Aug. 2022, Art. no. 102859, https://doi.org/10.1016/j.addma.2022.102859.

[14] C. Xu *et al.*, "Tailoring microstructure via heat treatment to improve the corrosion resistance of directed energy deposited nickel-aluminum bronze alloy," *Journal of Materials Research and Technology*, vol. 25, pp. 5210–5226, Jul. 2023, https://doi.org/10.1016/j.jmrt.2023.07.039.

[15] N. Tebbal, M. Maza, and Z. E. A. Rahmouni, "Use of a Full Factorial Design to Study the Relationship between Water Absorption and Porosity of GP and BW Mortar Activated," *Advances in Civil Engineering*, vol. 2022, no. 1, 2022, Art. no. 2016157, https://doi.org/10.1155/2022/2016157.

[16] S. S. M. Tavares, N. M. Mota, H. R. da Igreja, C. Barbosa, and J. M. Pardal, "Microstructure, mechanical properties, and brittle fracture of a cast nickel-aluminum-bronze (NAB) UNS C95800," *Engineering Failure Analysis*, vol. 128, Oct. 2021, Art. no. 105606, https://doi.org/10.1016/j.engfailanal.2021.105606.

[17] B. Zhang, J. Wang, J. Yuan, and F. Yan, "Tribocorrosion behavior of nickel-aluminium bronze sliding against alumina under the lubrication by seawater with different halide concentrations," *Friction*, vol. 7, no. 5, pp. 444–456, Oct. 2019, https://doi.org/10.1007/s40544-018-0221-y.

[18] S. Fooladi, F. Ashrafizadeh, M. A. Golozar, and S. A. Razavi, "Influence of Age Hardening on Mechanical Properties of Cast Nickel-Aluminum Bronze Containing Shrinkage Porosity," *Journal of Failure Analysis and Prevention*, vol. 19, no. 5, pp. 1498–1508, Oct. 2019, https://doi.org/10.1007/s11668-019-00757-0.

[19] D. Odabas, "Effects of Load and Speed on Wear Rate of Abrasive Wear for 2014 Al Alloy," *IOP Conference Series: Materials Science and Engineering*, vol. 295, no. 1, Jan. 2018, Art. no. 012008, https://doi.org/10.1088/1757-899X/295/1/012008.

[20] J. Kim, J. Kim, and C. Pyo, "Comparison of Mechanical Properties of Ni-Al-Bronze Alloy Fabricated through Wire Arc Additive Manufacturing with Ni-Al-Bronze Alloy Fabricated through Casting," *Metals*, vol. 10, no. 9, Sep. 2020, Art. no. 1164, https://doi.org/10.3390/met10091164.

[21] F. Halladj, A. Boukhiar, H. Amellal, and S. Benamara, "Optimization of Traditional Date Vinegar Preparation Using Full Factorial Design," *Journal of the American Society of Brewing Chemists*, vol. 74, no. 2, pp. 137–144, Apr. 2016, https://doi.org/10.1094/ASBCJ-2016-2188-01.

[22] N. T. Van and L. H. Ky, "The Influence of Plasma Nitriding Technology Parameters on the Hardness of 18ХГТ Steel Parts," *Engineering, Technology & Applied Science Research*, vol. 14, no. 2, pp. 13643–13647, Apr. 2024, https://doi.org/10.48084/etasr.7089.

[23] K. Touileb, A. Hedhibi, R. Djoudjou, A. Ouis, and M. L. Bouazizi, "Mixing Design for ATIG Morphology and Microstructure Study of 316L Stainless Steel," *Engineering, Technology & Applied Science Research*, vol. 9, no. 2, pp. 3990–3997, Apr. 2019, https://doi.org/10.48084/etasr.2665.

[24] J. Patel and D. Mori, "Application of 32 Full Factorial Design and Desirability Function for Optimizing The Manufacturing Process for Directly Compressible Multi-Functional Co-Processed Excipient," *Current Drug Delivery*, vol. 17, no. 6, pp. 523–539, Jul. 2020, https://doi.org/10.2174/1567201817666200508094743.